

Finite-temperature semimetal-insulator transition on the honeycomb lattice

Minh-Tien Tran^{1,2} and Kazuhiko Kuroki³

¹*Institute of Physics, Vietnamese Academy of Science and Technology, P.O. Box 429, 10000 Hanoi, Vietnam*

²*Asia Pacific Center for Theoretical Physics, POSTECH, Pohang, Gyeongbuk 790-784, Republic of Korea*

³*Department of Applied Physics and Chemistry, University of Electron Communication, Chofu, Tokyo 182-8585, Japan*

(Received 23 January 2009; revised manuscript received 10 March 2009; published 31 March 2009)

A semimetal-insulator transition in the Hubbard model on the honeycomb lattice is studied by using the dynamical mean-field theory. Electrons in the honeycomb lattice resemble the Dirac electron liquid and for weak interactions the system is semimetal. With increasing the local interaction, a semimetal-insulator transition occurs. We find a nonanalytical structure of the phase transition which consists of a first-order transition line ending in a second-order transition point and high-temperature crossover line. A phase separation of semimetal and insulator occurs at low temperatures. Maxwell construction is performed to determine the first-order transition line. The phase diagram is also presented.

DOI: [10.1103/PhysRevB.79.125125](https://doi.org/10.1103/PhysRevB.79.125125)

PACS number(s): 71.27.+a, 71.30.+h, 71.10.Fd

I. INTRODUCTION

The study of correlation driven metal-insulator transition (MIT) has attracted great attention in recent years. The MIT is realized in a number of transition-metal oxides and organic compounds by application of the pressure or chemical substitutions.¹ Far from the transition point, the metallic phase is well described by the Fermi-liquid theory while in the insulating phase the electrons are localized. When the magnetic frustration is large, the MIT occurs in the paramagnetic phase. The metallic state is a Fermi liquid with a renormalized mass. The renormalized mass increases as the transition is approached. This is the essence of the Brinkman-Rice theory of the MIT.² The Brinkman-Rice scenario of the MIT is substantially developed by the dynamical mean-field theory (DMFT) of the Hubbard model in the paramagnetic phase.³⁻⁵ The essential features of the MIT studied within the DMFT is a nonanalytical structure of the phase transition, which consists of the first-order transition line ending in a second-order transition point and the high-temperature crossover line.⁵⁻⁷ The nonanalytical structure of the MIT has been observed experimentally,⁸ as well as has been confirmed by cluster DMFT (Refs. 9 and 10) and by other techniques.¹¹

Recently, the experimental realization of a single layer of graphite, known as graphene,^{12,13} has brought up renewed interest in the low-temperature physics of the electrons on the honeycomb lattice. In the honeycomb lattice at half filling the noninteracting Fermi surface collapses into the edge points of the Brillouin zone. The tight-binding dispersion exhibits the Dirac cone near these points and the density of states (DOS) at the Fermi level vanishes. The electrons on the honeycomb lattice closely resemble one of the massless Dirac fermions in 2+1 dimensions. In particular, the Hubbard model on the honeycomb lattice can be considered as an asymptotic infrared massive quantum electron dynamics in 2+1 dimensions.¹⁴ Therefore, the electrons on the honeycomb lattice provide a condensed matter analogy of relativistic physics of electrons.

The honeycomb lattice is also a basis structure of a number of materials such as magnesium diboride¹⁵ or layered nitride superconductors.¹⁶⁻¹⁸ Electron correlations constitute

the essential properties of these materials such as unconventional superconductivity.^{19,20} The emergence of electron correlations and the specific features of the honeycomb lattice structure underlies the material properties. The Hubbard model on the honeycomb lattice is a minimal model to describe the emergence of electron correlations in the specific lattice structure.

For weak local interactions the electrons on the honeycomb lattice always stay in the paramagnetic state. There is no presence of superconducting or magnetic instabilities at weak coupling.¹⁴ The interaction only renormalizes the Fermi velocity. With increasing the local interaction, the renormalized velocity decreases. When the renormalized velocity vanishes, the electrons are localized and the state is insulating.²¹ It is a scenario of the semimetal-insulator transition (SMIT) on the honeycomb lattice. The transition occurs in the paramagnetic phase, and it is a version of the Mott MIT. However, due to the absence of the quasiparticle mass, the Brinkman-Rice scenario of the MIT cannot be applied to the honeycomb lattice. Parallel to the SMIT, at low temperatures the local interaction in the honeycomb lattice can lock electrons with different spins into the different sublattices that create a magnetic long-range order. The numerical simulations also find a semimetal-antiferromagnetic insulator transition (SMAFIT) on the honeycomb lattice at low temperatures.²²⁻²⁴ This transition is a type of the Slater MIT which is driven by long-range order. In the honeycomb lattice the Mott and the Slater MIT compete with each other. However, when the magnetic frustration is strong they can destroy the magnetic long-range order, and there is only the Mott transition. The previous DMFT studies of the SMIT on the honeycomb lattice showed that the SMIT is a second-order transition in the paramagnetic phase,^{21,25} whereas the variational calculations showed a first-order transition characteristic of the SMIT.²³ In this paper we reexamine the SMIT on the honeycomb lattice by the DMFT. We find a nonanalytical structure of the SMIT on the honeycomb lattice which has not been pointed out in the previous DMFT studies.^{21,25} The nonanalytical structure is reminiscent to the phase structure of the MIT in the square or the Bethe lattices where the DOS at the Fermi level is finite.⁵⁻⁷ It also consists of the first-order transition line ending in a second-order

transition point and the high-temperature crossover line. However, in contrast to the square or the Bethe lattices, the SMIT on the honeycomb lattice does not accompany the appearance and the disappearance of a quasiparticle peak at the Fermi level. The absence of a quasiparticle state at the Fermi level is a specific feature of the electron dynamics in the honeycomb lattice. The SMIT on the honeycomb lattice is accompanied with the appearance and the disappearance of a pseudogap structure near the Fermi level.

The outline of the present paper is as follows. In Sec. II we describe the DMFT for the Hubbard model in the honeycomb lattice. Numerical results are presented in Sec. III. In Sec. IV conclusion and remarks are presented.

II. MODEL AND METHOD

We consider the Hubbard model on the honeycomb lattice. The Hamiltonian of the system is

$$H = -t \sum_{\langle i,j \rangle, \sigma} c_{i\sigma}^\dagger c_{j\sigma} - \mu \sum_i c_{i\sigma}^\dagger c_{i\sigma} + U \sum_i n_{i\uparrow} n_{i\downarrow}, \quad (1)$$

where $c_{i\sigma}^\dagger$ and $c_{i\sigma}$ are the creation and the annihilation operator of electrons at site i with spin σ . $n_{i\sigma} = c_{i\sigma}^\dagger c_{i\sigma}$ is the density operator and t is the hopping integral between nearest-neighbor sites i and j . We will take t as the unit of energy. U is the local interaction and μ is the chemical potential. In the following we will consider only the half filling case, i.e., $\mu = U/2$. The honeycomb lattice has a specific feature in the band structure, where the Fermi surface of noninteracting electrons at half filling is just the edge points of the Brillouin zone. The tight-binding dispersion near these points exhibits the Dirac cone such as the relativistic electrons, and the DOS at the Fermi level vanishes. The noninteracting electron on the honeycomb lattice is a semimetal which has a zero gap at the Fermi level. The specific feature distinguishes the honeycomb lattice from other lattices such as the square or the Bethe lattices where the DOS at the Fermi level is finite. Apparently, in the honeycomb lattice the concept of effective mass is not appropriate to describe the electron properties. As a consequence, the standard description of the Mott MIT is not valid in the honeycomb lattice. To reveal the nature of the SMIT in the honeycomb lattice we use the DMFT.³⁻⁵ The DMFT is exact in infinite dimensions. However, for two-dimensional lattices, the DMFT neglects nonlocal correlations. The cluster DMFT studies for a square lattice have shown that the key features of the MIT are already captured by the single-site DMFT.¹⁰ Thus, one can expect a similarity for the honeycomb lattice.

Since the honeycomb lattice is a Bravais lattice with a basis of two lattice sites, the electron Green's function can be written in the form of matrix 2×2 ,

$$\mathbf{G}(\mathbf{k}, i\omega_n) = [\mathbf{G}_0^{-1}(\mathbf{k}, i\omega_n) - \Sigma(\mathbf{k}, i\omega_n)]^{-1}, \quad (2)$$

where $\omega_n = (2n-1)\pi T$ is the Matsubara frequency, $\Sigma(\mathbf{k}, i\omega_n)$ is the self energy, and $\mathbf{G}_0(\mathbf{k}, i\omega_n)$ is the bare Green's function of noninteracting electrons. The bare Green's function is

$$\mathbf{G}_0^{-1}(\mathbf{k}, i\omega_n) = \begin{pmatrix} i\omega_n + \mu & -\varepsilon(\mathbf{k}) \\ -\varepsilon^*(\mathbf{k}) & i\omega_n + \mu \end{pmatrix}, \quad (3)$$

where $\varepsilon(\mathbf{k}) = -2t \exp(ik_x/2) \cos(\sqrt{3}k_y/2) - t \exp(ik_x)$. Equation (2) is just the Dyson equation. Within the DMFT, the self energy is approximated by a local function of frequency, i.e.,

$$\Sigma(\mathbf{k}, i\omega_n) \approx \delta_{\alpha\beta} \Sigma(i\omega_n). \quad (4)$$

Note that within the DMFT the off diagonal elements of the self energy are neglected. These elements vanish in infinite dimensions. In finite dimension lattices they are indeed non-local correlation quantities. The self energy $\Sigma(i\omega_n)$ is determined from the dynamics of single-site electrons embedded in an effective mean-field medium. Once the effective single-site problem is solved, the self energy is calculated by the Dyson equation

$$\Sigma(i\omega_n) = \mathcal{G}^{-1}(i\omega_n) - G^{-1}(i\omega_n), \quad (5)$$

where $\mathcal{G}(\omega)$ is the bare Green's function of the effective single site and represents the effective mean-field acting on the site. $G(\omega)$ is the electron Green's function of the effective single site. The self-consistent condition requires that the Green's function $G(\omega)$ of the effective single site must coincide with the local Green's function of the original lattice, i.e.,

$$G(i\omega_n) = \frac{1}{N} \sum_{\mathbf{k}} G_{\alpha\alpha}(\mathbf{k}, i\omega_n), \quad (6)$$

where N is the number of lattice sites. Equations (2)–(6) form the self-consistent system of equations for the lattice Green's function and the self energy. They are principal equations of the DMFT. In order to solve the effective single-site problem we use the exact diagonalization technique.^{5,26} The exact diagonalization maps the effective single-site problem into an Anderson impurity model,

$$H_{\text{AIM}} = \sum_{p\sigma} E_p b_{p\sigma}^\dagger b_{p\sigma} + \sum_{p\sigma} V_p (b_{p\sigma}^\dagger c_\sigma + \text{h.c.}) - \mu c_\sigma^\dagger c_\sigma + U n_\uparrow n_\downarrow, \quad (7)$$

where the local impurity represented by c_σ^\dagger , c_σ couples to a bath of free conduction electrons represented by $b_{p\sigma}^\dagger$ and $b_{p\sigma}$ with dispersion E_p via a hybridization V_p . In the exact diagonalization the effective-medium Green's function $\mathcal{G}(i\omega_n)$ is approximated by the corresponding Green's function $\mathcal{G}_{n_s}(i\omega_n)$ calculated within the Anderson impurity model of a finite number of bath levels,

$$\mathcal{G}_{n_s}(i\omega_n)^{-1} = i\omega_n + \mu - \sum_{p=2}^{n_s} \frac{|V_p|^2}{i\omega_n - E_p}, \quad (8)$$

where $n_s - 1$ is the number of bath levels. The model parameters E_p and V_p are determined by minimization of the distance function,

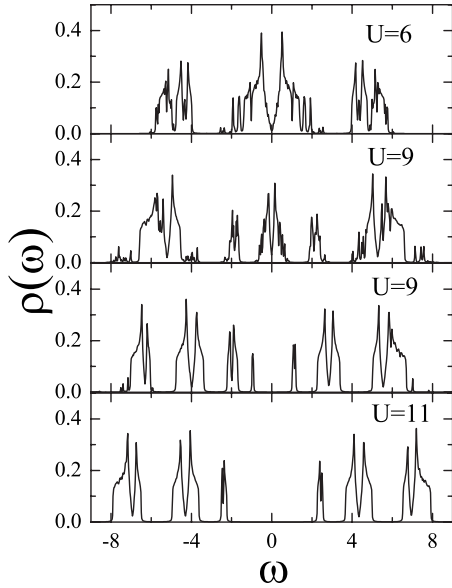


FIG. 1. Density of states $\rho(\omega)$ for various U at temperature $T=0.01$. The first two top panels plot the semimetal solution while the last two panels plot the insulator solution.

$$d = \frac{1}{M} \sum_{n=1}^M |\omega_n|^{-k} |\mathcal{G}(i\omega_n)^{-1} - \mathcal{G}_{n_s}(i\omega_n)^{-1}|^2. \quad (9)$$

If the parameter k is chosen, large ($k > 1$) enhances the importance of the lowest Matsubara frequencies in the minimization procedure. In particular, we take $k=3$ in the following numerical calculations. When the model parameters E_p and V_p are obtained we solve the Anderson impurity model by the exact diagonalization and obtain the local Green's function $G(i\omega_n)$ and then the self-energy $\Sigma(i\omega_n)$. Thus, we obtain a closed self-consistent system of equations for determining the electron Green's function within the DMFT.

III. NUMERICAL RESULTS

We solve the DMFT equations by iterations.^{5,26} Most calculations are performed with $M=1024$ positive Matsubara frequencies and the lattice size of 64×64 sites. For very low temperature (for instance $T=0.005$) we take $M=2048$. The exact diagonalization of the Anderson impurity model is performed with $n_s=7$. We have checked the agreement between $\mathcal{G}(i\omega_n)$ and $\mathcal{G}_{n_s}(i\omega_n)$ and found a good agreement for whole model parameter range under consideration. We find two typical solutions, one is semimetal and the other is insulator. The DOS of these solutions is presented in Fig. 1. The semimetal solution is characterized by a pseudogap near the Fermi level, while the insulator solution opens a wide gap at the Fermi level. In the semimetallic phase the DOS shows two Hubbard subbands and the pseudogap structure between them. In contrast to the square or the Bethe lattices, no Kondo quasiparticle peak appears at the Fermi level. In the honeycomb lattice, the DOS of noninteracting electrons linearly vanishes at the Fermi level, so that the Kondo-singlet formation resulted in the effective single-site problem is

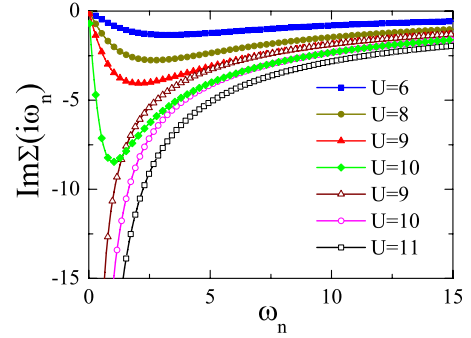


FIG. 2. (Color online) The imaginary part of the self energy for various interactions U at temperature $T=0.01$. The filled symbols are the self energy in the semimetallic phase, while the open symbols are the self energy in the insulating phase.

suppressed.²⁷ The feature of the noninteracting DOS is retained in the interacting case, so that the relativistic properties of the electrons in the honeycomb lattice are maintained as far as the system does not approach the SMIT. The local interaction only renormalizes the Fermi velocity which can be seen by the increase in the slope of the DOS near the Fermi level when the interaction increases. When the slope of the DOS near the Fermi level becomes very large, it closes the pseudogap and the system transforms to the insulating phase. At the point of the SMIT, the pseudogap structure disappears and leaves a wide gap in the DOS. In the insulating phase, the DOS exhibits only two Hubbard subbands separated by the gap. The SMIT scenario in the honeycomb lattice is reminiscent to the MIT in the square or the Bethe lattices. The crucial different feature is the absence of the Kondo quasiparticle state at the Fermi level in the honeycomb lattice. As a consequence, the Brinkman-Rice scenario of a divergence of the effective mass at the transition point is not valid. Instead, in the honeycomb lattice, the renormalized Fermi velocity vanishes when the system crosses the transition point. This SMIT scenario was also observed in the DMFT studies with the iterated perturbation theory as the impurity solver.²¹ However, at finite temperature we observe a coexistence of the semimetallic and the insulating solutions at intermediate interactions which has not been pointed in the previous DMFT studies.^{21,25}

In Fig. 2 we present the imaginary part of the self energy for various interactions in both the semimetallic and the insulating phases. The slope of $\text{Im}\Sigma(i\omega)$ for $\omega \rightarrow 0$ is identical to the slope of $\text{Re}\Sigma(\omega+i0^+)$ for $\omega \rightarrow 0$. The renormalized factor of the Fermi velocity is

$$Z = \frac{1}{1 - \left. \frac{\partial \text{Re}\Sigma(\omega+i0^+)}{\partial \omega} \right|_{\omega=0}}. \quad (10)$$

Figure 2 shows that in the semimetallic phase $\text{Im}\Sigma(i\omega) \rightarrow 0$ as $\omega \rightarrow 0$. It leads the DOS to be vanished at the Fermi level. As the interaction increases, the slope of $\text{Im}\Sigma(i\omega)$ for $\omega \rightarrow 0$ increases, so that the renormalized factor Z gradually decreases. When the system transforms to the insulating phase, the renormalized factor Z vanishes. Apparently, in the

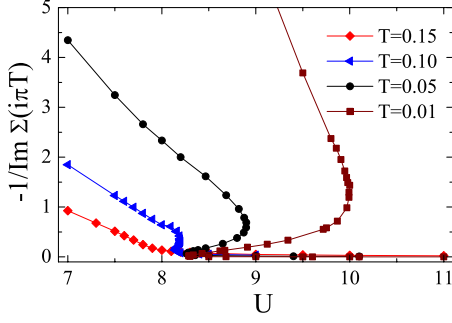


FIG. 3. (Color online) The quantity $Q = -1/\text{Im}\Sigma(i\pi T)$ as a function of U at different temperature T .

insulating phase the concept of the Fermi velocity is not valid and the use of Eq. (10) does not make sense. Nevertheless, at the SMIT point, the slope of $\text{Im}\Sigma(i\omega)$ for $\omega \rightarrow 0$ abruptly changes from a negative large value to a positive large value. It is a specific feature of the SMIT in the honeycomb lattice. In the square or the Bethe lattices, the slope of $\text{Im}\Sigma(i\omega)$ for $\omega \rightarrow 0$ continuously changes as the system crosses the MIT.⁵⁻⁷

At low temperatures we have found the insulator solution for $U > U_{c1}(T)$ and the semimetal solution for $U < U_{c2}(T)$. In the range $U_{c1}(T) < U < U_{c2}(T)$ both insulator and semimetal solutions coexist. The nonanalytical structure in the honeycomb lattice is very similar to the one in the square or the Bethe lattices.⁵⁻⁷ This suggests that the SMIT in the honeycomb lattice is a first-order transition. In order to reveal the nonanalytical structure of the phase transition we use the method proposed by Tong *et al.*²⁸ It is based on the observation that for a fixed temperature the formal dependence of a thermodynamical quantity Q on the interaction U is a multivalued function $h_Q(U)$. Usually, $h_Q(U)$ has a Z-shaped or S-shaped structure. The signal of the nonanalytical structure is the discontinuity of $Q(U)$ in the normal calculations. To obtain the multivalued function $h_Q(U)$, instead of $Q = h_Q(U)$ we transform it to a self-consistent equation,

$$Q = h_Q(U - \lambda[A - Q]), \quad (11)$$

where λ and A are parameters which are chosen so that Q is single valued with respect to U even if the original $h_Q(U)$ is a multivalued function. Equation (11) is embedded into the DMFT self-consistent equations. In the following calculations we take $Q = -1/\text{Im}\Sigma(i\pi T)$ which is the inverse of the imaginary part of the self energy at the first Matsubara frequency. This quantity is proportional to $\text{Im}\Sigma(i\omega_1)/\omega_1 \approx \partial \text{Re}\Sigma(\omega)/\partial \omega|_{\omega \rightarrow 0}$, which is a renormalized contribution to the Fermi velocity. In Fig. 3 we present Q as a function of U at various temperatures. One can see the Z-shaped structure of $h_Q(U)$ at low temperatures. At high temperatures $h_Q(U)$ is a single-value function. In the insulating phase Q vanishes, while in the semimetallic phase it is finite. The vanishing of Q also indicates the vanishing of the renormalized Fermi velocity. At low temperatures in the range $U_{c1}(T) < U < U_{c2}(T)$ we find an additional solution to the semimetal and the insulator solutions. An example of these three coexistent solutions are plotted in Fig. 4. One solution

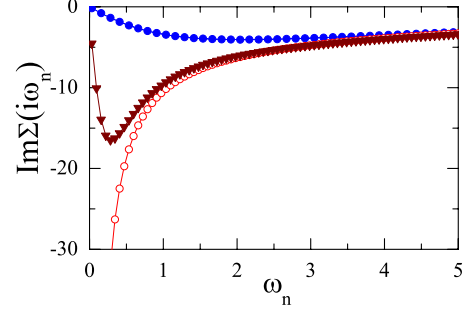


FIG. 4. (Color online) Three coexistent solutions at $U=9$ and $T=0.01$. The imaginary part of the self energy is plotted. The semimetal solution is presented by the blue filled circles, the insulator solution is presented by the red open circles, and the metastable solution is presented by the brown filled triangles.

is semimetal (filled circles) and the other is insulator (open circles). The additional solution (filled triangle) is found between them. It fills the positive slope piece of the multivalued function $h_Q(U)$. At high frequencies the additional solution closely approaches to the insulator solution, while at low frequencies it behaves like metallic. With the three coexistent solutions the function $h_Q(U)$ is continuous but multivalued in the region $U_{c1}(T) < U < U_{c2}(T)$, as can be seen in Fig. 3.

However, not all three solutions are stable. To find a stable solution we compare the free energies of the three coexistent solutions. The free energy can be calculated via the double occupation,²⁸

$$F(U, T) = F(0, T) + \int_0^U D(U', T) dU', \quad (12)$$

where $F(U, T)$ is the free energy and $D(U, T) = \langle n_\uparrow n_\downarrow \rangle$ is the double occupation. The double occupation can be calculated by the exact relation,²⁹

$$D = \frac{T}{U} \sum_n G(i\omega_n) \Sigma(i\omega_n) e^{i\omega_n 0^+}. \quad (13)$$

The double occupation is a measure of the portion of lattice sites which are occupied by electrons with both spins and characterizes the mobility degree of electrons in the lattice. For $U=0$, $D=0.25$, and for $U \rightarrow \infty$, $D=0$. The double occupation is often used to reveal the first-order phase transition.^{5,28} The DMFT shows that within a stable phase the double occupation decreases as U increases, and it exhibits a discontinuity when the system crosses a first-order transition line.^{5,28} Indeed, $D = \partial F / \partial U$ and $\partial D / \partial U = \partial^2 F / \partial U^2$. $\partial D / \partial U < 0$ shows a stability of phase. The variable pair $D - U$ is analogous to the inverse density and pressure in the conventional liquid-gas transition theory.^{28,30} In Fig. 5 we present the double occupation D as a function of U at various temperatures. It shows that the double occupation in the insulating phase is independent on temperature. It means that the thermal fluctuations do not affect the degree of the electron mobility in the insulating phase, because the gap strongly prevents the mobility of electrons. At high temperatures $D(U)$ is a single-value function, while at low temperatures $D(U)$ has a Z-shaped structure such as the quantity Q .

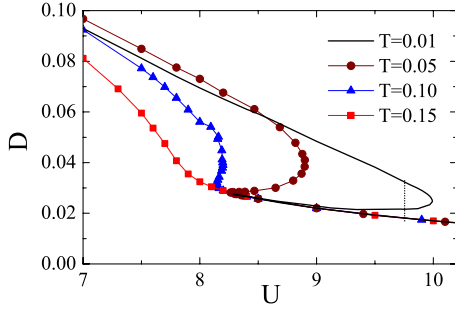


FIG. 5. (Color online) The double occupation D as a function of U at various temperatures. The solid line, filled cycles, triangles, and squares are the double occupation at temperature $T=0.01, 0.05, 0.1, \text{ and } 0.15$, respectively. The vertical dashed line is a Maxwell construction for $T=0.01$.

The obtained function $D(U)$ is very similar to the one in the square and Bethe lattices.²⁸ At high temperatures the double occupation $D(U)$ is smooth; thus, the system only crosses from semimetal to insulator. For low temperatures, at U_{c1} the double occupation $D(U)$ is continuous, but its slope is discontinuous. It means that the transition at U_{c1} is a second-order transition. At U_{c2} the double occupation is smooth; thus the system only crossovers from a semimetal to a metallic-like phase. However, comparing the free energy, one can see that the additional metallic-like phase has highest free energy, and therefore it is unstable. This feature is similar to the conventional liquid-gas transition, where the liquid and the gas phases coexist. The semimetallic phase is stable for $U < U_c(T)$, while the insulator one is stable for $U > U_c(T)$. $U_c(T)$ can be found by a Maxwell construction $F_{SM}(U_c, T) = F_I(U_c, T)$. At low temperatures as U crosses $U_c(T)$ from below, a stable semimetallic phase transforms into a stable insulating phase. This transition is accompanied with a finite jump ΔD of the double occupation, that it is a first-order transition. The finite low-temperature SMIT in the honeycomb lattice is of first order. When $T \rightarrow 0$, one can expect that $U_c \rightarrow U_{c2}$, and at U_c there is no jump of the double occupation. The zero-temperature SMIT in the honeycomb lattice is of second order.²¹ However, this second-order phase transition is special. It emerges from the metastable coexistent phases. At zero temperature near the phase transition a metastable phase still exists.

We summarize the results in the phase diagram presented in Fig. 6. At low temperatures the semimetallic phase persists up to $U_{c2}(T)$, while the insulating phase exists down to $U_{c1}(T)$. Both lines $U_{c1}(T)$ and $U_{c2}(T)$ terminate at the point U_{SMIT} . In the region $U_{c1}(T) < U < U_{c2}(T)$ three phases coexist. One phase is semimetallic, and the other is insulating. The third phase is unstable. Actually, the SMIT transition occurs along the line $U_c(T)$ which presents a first-order transition. The line $U_c(T)$ also terminates at the second-order transition point U_{SMIT} . In the region $U_{c1}(T) < U < U_c(T)$ the semimetallic phase is stable and the insulating phase is metastable, whereas in the region $U_c(T) < U < U_{c2}(T)$ the insulating phase is stable and the semimetallic phase is metastable. The phase separation is the essential feature of the SMIT on the honeycomb lattice. This is reminiscent of the MIT in the square or the Bethe lattices. The feature may be considered

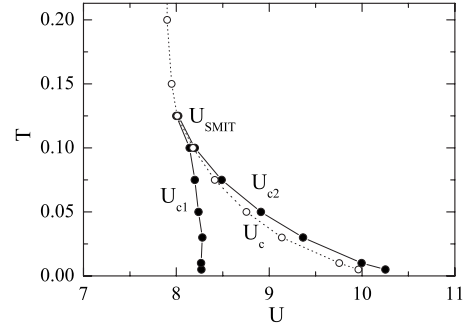


FIG. 6. Phase diagram of the SMIT in the honeycomb lattice.

as a common correlation effect regardless of the lattice structure. This may be unexpected because the MIT in the square or Bethe lattices is accompanied with the appearance and disappearance of a quasiparticle peak which is formed by the Kondo effect at the Fermi level. In the honeycomb lattice the Kondo effect is suspended and the Kondo quasiparticle peak at the Fermi level is absent. The SMIT on the honeycomb lattice is accompanied with appearance and disappearance of the pseudogap near the Fermi level. Apparently, the phase separation in the MIT is just an emergence of electron correlations in the boundary of metallic and insulating phases without involving a specific transition-driven mechanism. Near the zero temperature the first-order phase transition occurs at $U_c/t \approx 10$. The previous DMFT calculations adopting the iterated perturbation theory for single-site problem obtained $U_c/t = 13.3$ at $T=0$.²¹ It is well known that the iterated perturbation theory usually overestimates the critical value.³¹ The DMFT calculations for infinite dimension hyperdiamond lattice obtained $U_c/t \approx 8.5$.²⁵ In graphene samples,¹³ $U/t \sim 2-4$ is far from the SMIT. One may expect that the graphene is well described by the Dirac liquid theory with a renormalized velocity.

IV. CONCLUSION

In this paper we study the SMIT in the honeycomb lattice by using the DMFT. In contrast to the square or Bethe lattices, the SMIT in the honeycomb lattice occurs without involving the appearance and the disappearance of a quasiparticle state at the Fermi level. It is accompanied by the appearance and the disappearance of a pseudogap near the Fermi level. Far from the transition point the semimetallic phase is a Dirac electron liquid with a renormalized Fermi velocity, while in the insulating phase the electrons are localized. When the system approaches the SMIT point from below the renormalized Fermi velocity vanishes. We found a nonanalytical structure of the phase transition. It consists of a first-order transition line ending in a second-order transition point and high-temperature crossover line. At low temperatures the phase separation between the semimetallic and the insulating phases occurs. It suggests that the phase separation is a common feature of the Mott MIT regardless of a specific transition-driven mechanism. In two-dimensional lattices the DMFT neglects nonlocal correlations. The cluster DMFT calculations for a square lattice shows that the first-order

characteristic of the Mott MIT is already captured in the single-site DMFT.¹⁰ However, the nonlocal correlations modify the shape of the transition lines.¹⁰ One may expect the same feature in the honeycomb lattice. Moreover, in the honeycomb lattice the magnetic instability may compete with the Mott MIT at low temperatures. It requires further

study, at least, how strong short-range magnetic correlations affect the Mott MIT.

ACKNOWLEDGMENT

One of the authors (M.-T.T.) acknowledges the Nishina Memorial Foundation.

-
- ¹M. Imada, A. Fujimori, and Y. Tokura, *Rev. Mod. Phys.* **70**, 1039 (1998).
- ²W. F. Brinkman and T. M. Rice, *Phys. Rev. B* **2**, 4302 (1970).
- ³W. Metzner and D. Vollhardt, *Phys. Rev. Lett.* **62**, 324 (1989).
- ⁴A. Georges and G. Kotliar, *Phys. Rev. B* **45**, 6479 (1992).
- ⁵A. Georges, G. Kotliar, W. Krauth, and M. J. Rozenberg, *Rev. Mod. Phys.* **68**, 13 (1996).
- ⁶A. Georges and W. Krauth, *Phys. Rev. B* **48**, 7167 (1993).
- ⁷M. J. Rozenberg, G. Kotliar, and X. Y. Zhang, *Phys. Rev. B* **49**, 10181 (1994).
- ⁸P. Limelette, A. Georges, D. Jerome, P. Wzietek, P. Metcalf, and J. M. Honig, *Science* **302**, 89 (2003).
- ⁹O. Parcollet, G. Biroli, and G. Kotliar, *Phys. Rev. Lett.* **92**, 226402 (2004).
- ¹⁰H. Park, K. Haule, and G. Kotliar, *Phys. Rev. Lett.* **101**, 186403 (2008).
- ¹¹S. Onoda and M. Imada, *Phys. Rev. B* **67**, 161102(R) (2003).
- ¹²K. S. Novoselov, A. K. Geim, S. V. Morozov, D. Jiang, Y. Zhang, S. V. Dubonos, I. V. Grigorieva, and A. A. Firsov, *Science* **306**, 666 (2004).
- ¹³A. H. Castro Neto, F. Guinea, N. M. R. Peres, K. S. Novoselov, and A. K. Geim, *Rev. Mod. Phys.* **81**, 109 (2009).
- ¹⁴A. Giuliani and V. Mastropietro, arXiv:0811.1881 (unpublished).
- ¹⁵J. Nagamatsu, N. Nakagawa, T. Muranaka, Y. Zenitani, and J. Akimitsu, *Nature (London)* **410**, 63 (2001).
- ¹⁶H. Tou, Y. Maniwa, T. Koiwasaki, and S. Yamanaka, *Phys. Rev. Lett.* **86**, 5775 (2001).
- ¹⁷Y. Taguchi, M. Hisakabe, and Y. Iwasa, *Phys. Rev. Lett.* **94**, 217002 (2005).
- ¹⁸A. Kitora, Y. Taguchi, and Y. Iwasa, *J. Phys. Soc. Jpn.* **76**, 023706 (2007).
- ¹⁹G. Baskaran, *Phys. Rev. B* **65**, 212505 (2002).
- ²⁰S. Pathak, V. B. Shenoy, and G. Baskaran, arXiv:0809.0244 (unpublished).
- ²¹S. A. Jafari, arXiv:0809.1109 (unpublished).
- ²²S. Sorella and E. Tosatti, *Europhys. Lett.* **19**, 699 (1992).
- ²³L. M. Martelo, M. Dzierzawa, L. Siffert, and D. Baeriswyl, *Z. Phys. B: Condens. Matter* **103**, 335 (1997).
- ²⁴T. Paiva, R. T. Scalettar, W. Zheng, R. R. P. Singh, and J. Oitmaa, *Phys. Rev. B* **72**, 085123 (2005).
- ²⁵G. Santoro, M. Airoidi, S. Sorella, and E. Tosatti, *Phys. Rev. B* **47**, 16216 (1993).
- ²⁶M. Caffarel and W. Krauth, *Phys. Rev. Lett.* **72**, 1545 (1994).
- ²⁷K. Ingersent, *Phys. Rev. B* **54**, 11936 (1996).
- ²⁸N.-H. Tong, S.-Q. Shen, and F.-C. Pu, *Phys. Rev. B* **64**, 235109 (2001).
- ²⁹Y. M. Vilchik and A.-M. S. Tremblay, *J. Phys. I* **7**, 1309 (1997).
- ³⁰C. Castellani, C. Di Castro, D. Feinberg, and J. Ranninger, *Phys. Rev. Lett.* **43**, 1957 (1979).
- ³¹R. Bulla, T. A. Costi, and D. Vollhardt, *Phys. Rev. B* **64**, 045103 (2001).